**NASA TECHNICAL MEMORANDUM**

NASA TM X-71655

NASA TM X-71655



# DYNAMIC CHARACTERISTICS OF A 30-CM MERCURY ION THRUSTER

by John S. Serafini, Maris A. Mantenieks, and Vincent K. Rawlin
Lewis Research Center
Cleveland, Ohio 44135



TECHNICAL PAPER to be presented at
Eleventh Electric Propulsion Conference sponsored
by American Institute of Aeronautics and Astronautics
New Orleans, Louisiana, March 19-21, 1975

# DYNAMIC CHARACTERISTICS OF A 30-CENTIMETER MERCURY ION THRUSTER

J. S. Serafini, M. A. Mantenieks, and V. K. Rawlin
National Aeronautics and Space Administration
Lewis Research Center
Cleveland, Ohio



## Abstract

Measurements of the fluctuations of the discharge and beam plasmas of a 30-centimeter ion thruster have been performed using 60 Hertz laboratory type power supplies. The 30-centimeter thruster (modified 400 series) was operated at beam currents of 2.0, 1.5, and 1.0 amperes over a range of magnetic baffle currents, with the discharge power held at 183 eV/ion and discharge voltage at 37 volts. The time-varying properties of the discharge voltage and current, the ion beam current, and neutralizer keeper current were measured. The intensities of the fluctuations (ratio of the rms magnitude to time-average quantity) were found to depend significantly on the beam and magnetic baffle currents. The shape of the frequency spectra of the discharge plasma fluctuations was found to be related to the beam and magnetic baffle currents. The dependence on these time-average current levels was found to be complex. The predominant peaks of the beam and discharge current spectra occurred at frequencies less than 30 kilohertz. This discharge chamber resonance could be possibly attributable to ion-acoustic wave phenomena. Cross-correlations of the discharge and beam currents indicated that the dependence on the magnetic baffle current was strong. The measurements indicated that the discharge current fluctuations directly contribute to the beam current fluctuations and that the power supply characteristics can modify these fluctuations.

## Introduction

The 30-centimeter diameter ion thruster is being considered for primary propulsion applications for Earth orbital and interplanetary missions.[1-3] In these applications, electrical noise or fluctuations are of concern.[4,5] The operation of a mercury electron bombardment thruster can yield fluctuations about the mean current and potential of the ion beam, fluctuations of the discharge plasma, and fluctuations within the power conditioner itself. In addition, information on these fluctuations could aid in optimizing performance and life of the thruster and power supplies.

The present paper is a continuation of the work presented in Reference 6. The present work reports on measurements of the fluctuations in the beam current, neutralizer keeper current, discharge current, and discharge voltage. A range of beam current and magnetic baffle current values and discharge chamber conditions was covered in the investigation. Several properties of the fluctuations were recorded using the techniques of References 7 to 9. Included were the overall magnitude as given by the root-mean-square (rms) magnitude and the frequency spectral distribution. Cross-correlations were also obtained between (1) the beam fluctuations and the discharge current fluctuations, (2) the beam fluctuations and the neutralizer keeper current fluctuations and (3) the discharge current fluctuations and the discharge voltage fluctuations.

## Apparatus and Experimental Technique

### Thruster and Power Supplies

A 30-centimeter diameter mercury bombardment ion thruster built by Hughes Research Laboratories was used for the tests described herein. It was a "400 series" thruster modified to be nominally equivalent to the Engineering Model Thruster described in Reference 10 and the same thruster used in Reference 11. The cathode, the high-voltage isolator and the cathode vaporizer used consisted of a single assembly instead of the separated components of the ETM. Dished ion optics, a stronger magnetic field, and a shortened cathode pole piece and baffle mounts were also added to the "400 series" thruster. Also, the magnetic baffle control coil had $3\frac{1}{2}$ turns. The baffle diameter used was 5.08 centimeters except when otherwise mentioned. The thruster was operated in the 3.0 meter diameter port of the 7.6 meter diameter by 21.4 meter long vacuum facility at Lewis Research Center.[12]

Laboratory type power supplies powered from the 60 Hertz line were used to operate the thruster. Alternating current was used for all of the heaters. The discharge supply output was of a full wave rectified transformer type with a $\pi$ filter using two 4000 microfarad capacitors and a 6 millihenry choke. A series transistor current regulator was inserted after the filter. The keeper discharge supplies used ballast resistors to limit the output current. The beam current and discharge voltage were each held at selected values through the use of feedback control loops which controlled the power to the main and cathode vaporizers, respectively.

### Thruster Operation

The thruster was always operated with net and total accelerating voltages of 1100 and 1600 volts, respectively. The discharge losses were fixed at 185 electron volts per beam ion for all beam currents. The beam current was varied by adjusting the main propellant flow to the thruster and beam currents of 1.0, 1.5, and 2.0 amperes were used in the tests. The discharge voltage was maintained constant at 37.0 volts by adjusting the mercury flow through the cathode. For any given set of thruster electrical operating conditions, the cathode flow rate could be increased by increasing the current through the magnetic baffle control coil.[13] The values of magnetic baffle current chosen (up to 15 A) allowed stable thruster operation. For the entire series of tests the neutralizer was operated at a constant keeper current of 2 amperes with a flow rate of approximately 60 milliamperes.

### Transducers and Calibration

Three current transformer probes were used to sense the discharge current, beam current, and neutralizer keeper current fluctuations (time-varying component of the current). These probes were placed around the appropriate current-carrying con-

ductors from the power supplies to the thruster. The discharge voltage fluctuations were measured by using a current probe to sense the current through a 1000 ohm noninductive resistance connected across the discharge supply leads. The sensitivity of the current probes ranged from 0.5 to 0.1 volt per ampere. The saturation to d.c. current was well above the measured levels.

The probes were checked for gain and frequency response and were found to have a flat response over the frequency range reported herein (100 Hz to 450 kHz). Phase difference (of importance in the correlation studies as described in Ref. 6) between the output signals for the two probe systems was negligibly small over the frequency range of interest. For further details on the calibration of the data system refer to Figure 1 and Reference 6.

Analysis of Time-Varying Data

The magnitude of the time-varying output signals from the current probe systems was measured on true rms meters. The amplitude as a function of frequency was measured by the use of three spectrum analyzers. The signals from the spectrum analyzers were plotted by X-Y recorders. Cross-correlation and auto-correlation functions of the fluctuations were also generated. A brief description of this technique and its implications are given in Appendix B of Reference 6.

## Results and Discussion

This section will present the results of the rms magnitude, spectral data, and correlation measurements in that order.

RMS Magnitudes

Figure 2 shows the fluctuation intensity, the ratio of the rms magnitude to the time-average currents (see Appendix A - List of Symbols) for the beam current and discharge voltage and current as a function of $J_{MB}$, the magnetic baffle current, for a $J_B$ of 2.00 amperes, $\Delta V_I$ of 37.0 volts, and a $J_I$ of 12.0 amperes. The lowest value of $J_{MB}$ in Figure 2 (6.0 A) was the lowest value at which the thruster subsystem could be operated stably.

Ordinarily, to study the behavior of the discharge chamber plasma, the emission current $J_E(t)$ is sensed. As it was not convenient to sense the emission current fluctuation, the anode and beam current fluctuations were sensed instead. The validity of this procedure was checked by observing the discharge chamber plasma fluctuations with the beam on and off. A further discussion of the validity of sensing the fluctuations of $J_I$, the discharge current, rather than those of $J_E$, the emission current is given in Appendix B.

The behavior of the fluctuation intensity as a function of $J_{MB}$ suggests that several different plasma modes are experienced over this range of $J_{MB}$. Further information on this point will be discussed subsequently in the section on spectral data. Similar behavior of the fluctuation intensities as a function of $J_{MB}$ were found in Reference 6 which further emphasizes the possibility that over this range of $J_{MB}$ there exists several plasma modes. The shapes of the curves presented here are similar to those of Reference 6 but are not identical. The lack of identity might possibly be attributed to the differences in the interactions of the thruster plasmas with their power supplies or the differences in discharge chamber geometry and magnetic field. For the work reported in Reference 6, the thruster (a "4000 series"), modified only by the addition of dished ion optics, was powered by a high-frequency transistor inverter type console.

In Figure 2 the fluctuation intensity curves for the discharge current and voltage are nearly identical while the curve for the beam fluctuations has a magnitude considerably lower than the other two curves over the measured range of $J_{MB}$. The intensity of the discharge current and beam current fluctuations are lower than those given in Reference 6.

It is of interest to examine the behavior of the fluctuation intensities as a function of cathode flow rate. In order to present this type of data the cathode flow-rate was measured as a function of the magnetic baffle current and the results are presented in Figure 3 for beam currents of 2.0, 1.5, and 1.0 amperes. While it was known that at constant $\Delta V_I$ increasing the magnetic baffle current resulted in an increase of cathode flow rate,[11,13] the behavior exhibited in Figure 3 which shows an apparent break or transition in the curves had not been observed previously.

Using the data of Figure 3 allows the presentation of the fluctuation intensities as a function of cathode flow rate. Figure 4 gives the fluctuation intensity for the discharge voltage and current and beam current as a function of $\dot{m}_c$, the equivalent cathode flow rate in milliamperes, for a $J_B$ of 2.0 amperes. Varying the $J_{MB}$ does change only slightly the magnetic field in the discharge chamber. However, the effect is strongest in the region of the baffle gap. This results in changing the effective resistance to the electrons emanating from the hollow cathode and directly affects the cathode flow rate at constant discharge voltage. From values of $\dot{m}_c$ of 65 milliamperes to approximately 100 milliamperes, there are relatively small changes in fluctuation intensities. This is especially significant when it is considered that, for optimum performance, the cathode flow rates are expected to be at these lower values.

The effect of varying the beam current on the fluctuation intensities as a function of $J_{MB}$ is given in Figures 5 and 6. Figure 5 compares the fluctuation intensity for the discharge current as a function of $J_{MB}$ for $J_B$ values of 1.0, 1.5, and 2.0 amperes. The variation of the fluctuation intensity with magnetic baffle current for $J_B$ values of 1.5 and 1.0 amperes is similar to that for a beam current of 2.0 amperes. The values of $J_{MB}$ at which the maxima occur increases as $J_B$ is increased. Near the maxima of the curves there was a low-frequency amplitude modulation of the fluctuation intensity. It was most severe for a $J_B$ value of 1.5 amperes. The range of values of the fluctuation intensity existing under these conditions is shown in Figure 5 by an error bar (±0.015) at $J_{MB}$ of 10 amperes ($J_B$ of 1.5 A curve).

Figure 6 compares the fluctuation intensity of the beam current, as a function of $J_{MB}$ for a $J_B$ of 1.0, 1.5, and 2.0 amperes. The effect of varying $J_B$ is generally similar to that observed in

Figure 5. As $J_{MB}$ is decreased to the minimum value, however, the beam current fluctuation intensity does not continue to decrease for $J_B$ of 1.5 and 1.0 amperes as in the case of $J_B$ of 2.0 amperes. In fact, for a $J_B$ of 1.5 amperes, the average value of the beam current fluctuation intensity at minimum $J_{MB}$ is 0.060 which is nearly as great as the maximum of the curve (0.064) occurring at a higher $J_{MB}$.

The effect on the fluctuations of varying the discharge current at beam currents of 2.0, 1.5, and 1.0 amperes is given in Figure 7. Given in the figure is the fluctuation intensity as a function of $\overline{J_I}$ for the fluctuations in beam current and discharge current and voltage. For all the data in the figure $\Delta V_I$ was constant at 37.0 volts. The values of magnetic baffle current, were 7.0, 7.5, and 8.0 amperes for $J_B$ of 2.0, 1.5, and 1.0 amperes, respectively. $J_I$ was varied around the nominal operating values for any given $J_B$, namely, a $J_I$ of 12.0, 9.0, and 6.0 amperes for $J_B$ of 2.0, 1.5, and 1.0 amperes, respectively. The behavior of the curves for the three beam currents is not similar. The levels of the intensities for $J_B$ of 1.5 amperes are higher than those for $J_B$ of 2.0 amperes, particularly in the case of the discharge voltage fluctuations. Examination of the fluctuations at a $J_B$ of 1.0 amperes reveals that (1) the shape of the curve and its variation with $\overline{J_I}$ is dissimilar to that found for $J_B$ values of 1.5 and 2.0 amperes and that (2) the intensity for the beam current fluctuations is much higher than those for $J_B$ of 1.5 and 2.0 amperes. In fact, at a $J_B$ value of 1.0 amperes, the fluctuation intensities of the beam current are about the same for those of the discharge current. From Appendix B it can be seen that this result is not due to measuring $J_I$ rather than $J_e$ fluctuations.

A parametric study was made of the effect of varying the discharge voltage (with all other thruster parameters maintained at their nominal operating values) and noting the fluctuations of the beam current, discharge voltage, and discharge current. The range of discharge voltage was varied from 36.0 to 38.0 volts. For the discharge current, the fluctuation intensity typically ranged from about 0.045 to 0.060. For the discharge voltage, the fluctuation intensity was essentially constant with values of 0.063, 0.087, and 0.094 for $J_B$ of 2.0, 1.5, and 1.0 amperes, respectively. For the beam current, the fluctuation intensity was essentially constant with values of 0.018 and 0.032 for $J_B$ of 2.0 and 1.5 amperes, respectively, and for a $J_B$ of 1.0 linearly ranged from 0.043 to 0.080.

The neutralizer keeper current and flow rate were not varied throughout the entire series of tests. With $\overline{J_{NK}}$, the time-average neutralizer keeper current, of 2.0 amperes, the fluctuation intensity, $j'_{NK}$, was 0.068±0.001.

Spectral Data

Two types of spectral data will be presented in this section. First in Figures 8 to 10 the amplitude spectra of the discharge current fluctuations are presented for $J_B$ values of 2.0, 1.5, and 1.0 amperes, respectively, for a range of values of $J_{MB}$. For this spectral data, the fundamental frequency, $F_0$, and the harmonic set of frequencies ($F_1$, $F_2$, $F_3$, . . .), along with their corresponding relative amplitudes ($A_0$, $A_1$, $A_2$, $A_3$, . . .), are summarized in Table 1. The second type of spectral data is given in Figure 11 which gives the relative log amplitude of the fluctuations of beam current, neutralizer keeper current, and discharge current and voltage as a function of frequency for a given thruster operating condition.

Figures 8(a) and (b) show the relative amplitude of the discharge current fluctuations as a function of frequency up to 50 kilohertz at a $J_B$ of 2.0 amperes for several values of $J_{MB}$. As the magnetic baffle current was varied from the minimum value of 6.0 amperes to 12.0 amperes, the cathode flow rate was also increasing in a manner discussed previously. Looking at the spectrum for any given value of $J_{MB}$ reveals that the spectrum up to 50 kilohertz has a number of peaks including a major one (always having a relative amplitude value of 1.0 by definition). Inspection of the spectrum for $J_{MB}$ of 6.0 in Figure 8(a) shows that the major peak does not occur at the lowest or fundamental frequency. It occurs at 15.6 kilohertz. There is a smaller peak at a frequency of 7.7 kilohertz. The oscillation is occurring at the first harmonic frequency not the fundamental and there also are smaller peaks at 23.0, 30.0, and 37.6 kilohertz which could be those occurring at the second, third, and fourth harmonic frequencies (Table 1(a)). For a $J_{MB}$ of 7.0 amperes in Figure 8(a) there is a similar behavior. For both curves of Figure 8(a) there are also other smaller peaks which are not included in this harmonic set.

The data for a $J_{MB}$ value of 8.5 amperes in Figure 8(b) reveals that the major peak occurs at a frequency of 19.3 kilohertz and a harmonic set now has only frequencies of 9.8 and 19.3 kilohertz corresponding to the zeroth and first harmonic frequencies, respectively. Peaks occurring at frequencies other than this harmonic set are plainly evident for this value of $J_{MB}$ and they occur at 5.0, 13.7, and 23.9 kilohertz. The curve for a $J_{MB}$ value of 12.0 amperes reveals that the major peak occurs at a frequency of 20.8 kilohertz and the harmonic set (as shown in Table 1(a)) now has frequencies of 10.2, 20.8, 32.0, and 43.0 kilohertz. Two points to note about the data for a $J_{MB}$ value of 12.0 amperes are (1) the lack of smaller peaks other than the harmonic set and (2) the fact that the third harmonic peak at 43.0 kilohertz has a large relative amplitude of 0.75.

Considering the frequencies of the major peaks in Figures 8(a) and (b) it is seen that they are 15.6, 18.0, 19.3, and 20.8 kilohertz for $J_{MB}$ of 6.0, 7.0, 8.5, and 12.0 amperes, respectively. This frequency increases nonlinearly with the $J_{MB}$.

Figures 9(a) and (b) show the relative amplitude as a function of frequency for the discharge current fluctuations at a $J_B$ value of 1.5 amperes for several values of $J_{MB}$. Figure 9(a) gives the data for $J_{MB}$ of 7.0 and 9.0 amperes and Figure 9(b) for $J_{MB}$ of 11.0 and 15.0 amperes. These spectra were selected as being representative of a larger number obtained over the range of $J_{MB}$ from 7.0 to 15.0 amperes. Inspection of the spectrum for $J_{MB}$ of 7.0 amperes in Figure 9(a) shows that the major peak does occur at the fundamental frequency, 10.3 kilohertz, of a harmonic set which consists of 10.3, 20.4, 30.3, and 41.2 kilohertz (Table 1(b)). For this $J_B$ value, at the minimum $J_{MB}$ value of 7.0 amperes, there is a significant

difference from the case where the $J_B$ equalled 2.0 amperes in not only the frequency at which the dominant peak occurs, but also in that there apparently is a mode change. This can be deduced from the shift in the major peak from the fundamental to the first harmonic frequency for the shift in $J_B$ from 1.5 to 2.0 amperes. This behavior with a change of $J_B$ implicitly involves $J_I$ as well. This is so because the energy expenditure per ion is kept constant as $J_B$ is varied. The effect of varying $J_I$ (and varying the energy expenditure per ion) with $J_B$ being held constant is considered later in this section.

Examination of the curve for a $J_{MB}$ value of 9.0 amperes in Figure 9(a) reveals that the major peak occurs at a frequency of 15.7 kilohertz and that the harmonic frequencies are not quite as well defined by distinguishable smaller peaks. In fact, although there are smaller peaks at frequencies of 4.5, 8.0, 19.5, 23.5, 31.0, and 39.5 kilohertz, this spectrum is so dominated by the main peak that an oscilloscope trace of the discharge current fluctuation probably would appear to be a very nearly sinusoidal function of time.

In Figure 9(b) the spectrum for $J_{MB}$ equal to 11.0 amperes is quite distinctive and is different from those previously shown. In this case there is a set of peaks with frequencies of 8.6, 17.0, 25.5, 33.8, and 42.3 kilohertz (Table 1(b)) with none of these peaks being small. In addition, the relative amplitude at frequencies less than 0.2 kilohertz is 0.48.

The spectrum for $J_{MB}$ equal to 15.0 amperes in Figure 9(b) is again significantly different from those previously discussed. Here two fairly broad peaks occur, the major one at a frequency of 20.9 kilohertz and a second one with a relative amplitude of 0.47 at a frequency of 41.7 kilohertz, the first harmonic. There are probably other harmonic frequencies greater than the 50 kilohertz limit of the figure. From the results presented in Figures 9(a) and (b) it is again seen that there are changes of modes of plasma fluctuations in the discharge chamber as the magnetic baffle current is varied.

Figure 10(a) gives the spectra of the discharge current fluctuations for $J_{MB}$ values of 8.0 and 9.0 amperes with $J_B$ at 1.0 amperes. For $J_{MB}$ of 8.0 amperes the major peak occurs at a frequency of 9.8 kilohertz with a first harmonic at a frequency of 19.4 kilohertz having a relative amplitude of 0.47 and with other smaller peaks occurring at 24.2, 29.2, and 38.8 kilohertz (Table 1(c)). In addition, the relative amplitude for frequencies below 0.2 kilohertz is 0.43. Looking at the spectrum for a $J_{MB}$ value of 9.0 amperes in Figure 10(a) reveals that the major peak now occurs at a frequency of 9.1 kilohertz (Table 1(c)). Other smaller peaks also occur at frequencies of 4.7, 13.5, 17.8, 22.3, 26.5, 31.2, and 35.6 kilohertz. The relative amplitudes are 0.56 and 0.55 for the peaks with the frequencies at 17.8 and 22.3 kilohertz, respectively. It is possible to interpret all of the observed peaks in this spectrum as a harmonic set, with the major peak occurring at the first harmonic.

Figure 10(b), which gives the spectra of the discharge current fluctuations for $J_{MB}$ values of 10.0, 12.0, and 15.0 amperes with $J_B$ held at 1.0 amperes, reveals a set of curves which have several unique features. The spectrum for a $J_{MB}$ value of 10.0 amperes in Figure 10(b) has peaks at frequencies of 6.3, 12.3, 18.7, and 30.0 kilohertz with the major peak being at 12.3 kilohertz (Table 1(c)). All of the peaks in this spectrum can be interpreted as a set of harmonic peaks with the major peak occurring at the first harmonic. Examination of the spectrum for $J_{MB}$ equal to 12.0 amperes in Figure 10(b) reveals that, in this case, all the peaks except one can be considered as a harmonic set. The peaks occur at frequencies of 4.7, 8.0, 14.5, 20.8, and 28.5 kilohertz (Table 1(c)). The major peak occurs at a frequency of 8.0 kilohertz. In this case the most likely set of harmonics is based on 8.0 kilohertz as the fundamental frequency.

Observing the spectrum with $J_{MB}$ at 15.0 amperes in Figure 10(b) reveals that the peaks are broader and that they occur at 6.7, 18.5, and 36.3 kilohertz with the major peak occurring at 18.5 kilohertz (Table 1(c)). In this case there are two possible harmonic set models. If the peak at a frequency of 6.7 kilohertz is ignored, the harmonic set is such that the fundamental frequency is at 18.5 kilohertz, the frequency of the major peak, with the first harmonic occurring at 36.3 kilohertz. On the other hand one can assume that the 6.7 kilohertz is the frequency of the fundamental and then the harmonic set consists of the zeroth, second, and fifth harmonics.

Spectral data for the fluctuations resulting from varying the discharge current and voltage was taken but will not be presented here. However, the behavior of the main peak of the spectra is considered. The discharge current, $J_I$, was varied over a range of ±10 percent about the $J_I$ values of 12.0, 9.0, and 6.0 amperes for $J_B$ of 2.0, 1.5, and 1.0 amperes, respectively. Over this range of variation, the frequency of the major peak was found to vary nonlinearly with $J_I$. The greatest variation in frequency was ±13 percent (from the frequency occurring at $J_I$ equal to 9.0 A) for a $J_B$ of 1.5 amperes. For a variation of the discharge voltage, $\Delta V_I$, of ±1 volt about 37 volts, the variation of the frequency of the major peak was found to be linear and was ±3 percent of the value of the frequency occurring at 37 volts.

The spectra in Figures 8, 9, and 10 have been presented and discussed in some detail to delineate clearly the complexity of the phenomena which occur for the several values of $J_B$ and ranges of $J_{MB}$ studied. Considerable analysis will be required to develop models adequately explaining both the details of these spectra and the fluctuation intensity results. Before even that can be done, however, additional information on the dynamics of the plasma in the ionization chamber will have to be obtained. It also will be necessary to analyze the dynamic characteristics of the power supplies for the thruster and to consider possible interactions of thruster and power supply.

Despite the complexity of the spectra, some possibilities as to their physical origin should be considered. Simple calculations reveal that, of the resonances or oscillations observed in similar plasmas, there are at least three possible mechanisms to examine.[14-16] These possibilities are

ion-acoustic resonances, resonances due to $\vec{E} \times \vec{B}$ particle drifts, and resonances due to effects of anomalous diffusion. Without a more complete knowledge of the plasma properties of 30-centimeter discharge chamber plasmas, it will not be possible to compare quantitatively the frequencies of observed peaks with the calculated values. However, by making some appropriate assumptions and estimates for the plasma parameters, at least a qualitative comparison can be presented.

The ion-acoustic resonance can be calculated by using $v_{th} = \sqrt{kT_e/M_I}$ for the characteristic velocity where $T_e$ is the electron temperature and $M_I$ is the mass of the mercury ion. A characteristic frequency is determined from $v_{th}/\ell$ where $\ell$ is a characteristic length in the discharge. If a $T_e$ of 5 electron volts[17] and an $\ell$ of 15 centimeters (half-diameter of the 30-cm thruster) are assumed, then the characteristic frequency obtained is 10.3 kilohertz. How $T_e$ varies with the operating conditions is not known. Also, the validity of the characteristic length assumption may be questioned. However, these estimates of the ion-acoustic resonant frequencies appear to be in reasonable argument with the results presented in Figures 8 to 10.

The $\vec{E} \times \vec{B}$ particle drift resonance can be calculated by using $v_D = 10^8 E/B$ for the characteristic velocity where E is in volts per centimeter and is assumed perpendicular to B given in gauss and $v_D$ is obtained in centimeters per second. A characteristic frequency can be calculated as $v_D/\ell$ where $\ell$ in centimeters is a characteristic length in the discharge. Assuming E, B, and $\ell$ being 0.2 volts per centimeter, 20 gauss, and 15 centimeters, respectively, gives 67 kilohertz as a characteristic frequency. This estimate probably represents a minimum value that could be expected for the $\vec{E} \times \vec{B}$ resonant frequency to exist. This is true because the average electric field (outside the sheaths) is probably higher than the above estimate and the value of average B lower. Therefore, the possibility that $\vec{E} \times \vec{B}$ particle drift resonance causes the observed peaks is remote.

A calculation of the plasma resonance resulting from anomalous diffusion[16] will not be attempted because of the complete lack of needed plasma parameters such as the ion temperature and the critical magnetic field at which there is an onset of the anomalous diffusion. In addition, geometry, interaction of the thruster plasma with the power processor and other factors may affect the resonance in the plasma but are not considered here.

Up to this point the spectra of the discharge current fluctuations have been shown only up to a frequency of 50 kilohertz. It is of interest to increase this range of frequencies and to compare the spectra of the fluctuations of the discharge current and voltage, the neutralizer keeper current and beam current. This is presented in Figure 11 which gives the spectra with the relative amplitude in decibels as a function of frequency in hertz (plotted on a log scale) for a range of frequencies to 450 kilohertz. The thruster operating conditions for the data of Figure 11 are: $J_B$ equal to 2.0 amperes, $J_I$ equal to 12.0 amperes, $\Delta V_I$ equal to 37.0 volts, and $J_{MB}$ equal to 7.0 amperes. This value of $J_{MB}$ at a $J_B$ of 2.0 amperes represents a stable mode of the thruster at a minimum cathode flow rate. Figure 11(a) gives the spectrum for the discharge current fluctuations. As previously noted, the main peak is at a first harmonic frequency of 18 kilohertz and there are other harmonic frequencies in evidence in consecutive order up to 81 kilohertz. Those peaks occurring at harmonic frequencies above 18 kilohertz decrease in amplitude such that at 81 kilohertz, the relative amplitude of the peak is -49.5 decibels.

There are several peaks at higher frequencies, specifically 187 and 379 kilohertz with the relative amplitudes being -50 and -69 decibels, respectively. This set of frequencies may be the fundamental and first harmonic frequencies of a resonance which is only of minor importance in the discharge chamber and is left unexplained. The relative amplitude at frequencies from 100 to 200 hertz is about -20 decibels and may be indicative of the effect of the power supply low frequency ripple on the fluctuations of the discharge chamber plasma. No such indication was found in Reference 6 which presents a spectrum of the discharge current fluctuations, taken with $J_B$ at 2.0 amperes and $J_{MB}$ at 13.0 amperes. The power conditioning console used contained 10 and 5 kilohertz inverters rather than 60 hertz laboratory supplies. In Reference 6 for frequencies greater than the main-peak frequency, the fall-off in amplitude with increasing frequency was found to be 45 decibels per decade. Because of the multiplicity of peaks in Figure 11(a) the fall-off in amplitude with increasing frequency is determined by a locus of the minima between the peaks. This gives a slope of about -48 decibels per decade. This reasonable agreement with Reference 6 suggests that the power supply differences may not be important at the higher frequencies for the fluctuations in discharge current.

Figure 11(b) presents the spectrum of the fluctuations of the discharge voltage. Its shape is generally similar to that for the discharge current fluctuations. The spectrum in Figure 11(b) has, as expected, a similar set of peaks at the same frequencies as Figure 11(a). For frequencies greater than the main-peak frequency, the fall-off in amplitude with increasing frequency is about 32 decibels per decade which is considerably less than that for the discharge current fluctuations. Also, in Figure 11(b) even at frequencies greater than 100 kilohertz there is evidence of a modulation of the relative amplitude in frequency intervals of approximately 5 kilohertz.

The spectrum of the neutralizer keeper current fluctuations is given in Figure 11(c). The main peak of this spectrum is in the 100 to 200 hertz frequency range. The next highest peak has a relative amplitude of -38 decibels and is at 17.5 kilohertz. In Reference 6, the spectrum of the neutralizer keeper current fluctuations consisted entirely of discrete peaks of a harmonic set with the fundamental frequency being 5.4 kilohertz, the inverter frequency. Thus, these two spectra are quite dissimilar.

Figure 11(d) presents the spectrum of the beam current fluctuations. The main peak is at a frequency of 18 kilohertz and, as was found for the discharge chamber fluctuations in Figures 11(a) and (b), can be considered as the first harmonic of a harmonic set. In evidence in Figure 11(d) is the peak at 180 kilohertz with a relative amplitude of

-59 decibels. Similar peaks were observed in the spectra of the discharge voltage and current fluctuations. At frequencies greater than the main-peak frequency the fall-off in relative amplitude with increasing frequency is -48 decibels per decade. Thus, the spectrum of the beam fluctuations appears to depend on the spectrum of the discharge chamber fluctuations. In addition the spectrum of the beam fluctuations appears to depend on the neutralizer fluctuations in the lower frequency range. Looking at the low frequency part of Figure 11(d) it is seen that the relative amplitude is as high as -9 decibels and this appears to be related to the main peak of the spectrum of the neutralizer keeper current fluctuations. The apparent dependence of the beam fluctuation spectra on the discharge fluctuations is a result also found in Reference 6. Although the spectra of the neutralizer keeper current fluctuations are dissimilar in Figure 11(c) and Reference 6, in both cases there is an effect on the beam fluctuation spectra.

Because the size of the baffle used has a strong effect on the $J_{MB}$ cathode flow rate relation, it should be expected to alter not only the time-average discharge characteristic but also the time-varying properties of the discharge. Figure 12 compares the spectra of discharge current fluctuations for baffle diameters of 5.08 and 5.72 centimeters. Preceding results have been presented for the 5.08 centimeter diameter baffle as a dashed curve in Figure 12 and is taken from Figure 11(a). The solid curve presents data for the 5.72 centimeter diameter baffle at $J_{MB}$ of zero and $J_B$ of 2.0 amperes (both curves represent a stable, low cathode flow rate). This comparison in Figure 12 illustrates clearly the significant change in the spectrum of the discharge fluctuations that can result from the slight change in baffle size. In the case of the spectrum for the 5.72 centimeter baffle diameter, the set of peaks contains only two with frequencies at 29 kilohertz and 78 kilohertz. The lower peak may be a second harmonic of the higher one. However, the frequency ratio is 2.7. Because the error in determining the frequency is hardly sufficient to say 2.7 is equivalent to 3.0, these two peaks are probably the result of two different physical resonance phenomena. Both peaks are broader than for those with the smaller size baffle. The fall-off in amplitude at the higher frequencies is about 65 decibels per decade for the larger baffle diameter. This is a significantly greater fall-off than was obtained for the smaller baffle size as in Reference 6.

## Correlations of the Fluctuations

A limited set of cross-correlations of the thruster fluctuations was obtained (see Appendix B for definition and discussion of cross-correlations). Correlation curves were obtained in terms of R, the correlation coefficient, as a function of $\tau$, the time delay between the fluctuations. Figure 13 presents $R_{max}$, the maximum correlation coefficient, as a function of $J_{MB}$, the magnetic baffle current, for a $J_B$ equal to 2.0 amperes. The solid curve in Figure 13 is for the cross correlation of the fluctuations of discharge voltage and current. As the magnetic baffle current is varied from 6.0 to 12.0 amperes, there is a rather slight variation in $R_{max}$ over a significant range of $J_{MB}$. Also, the values of $R_{max}$ are rather high ($R_{max}$ equal to 1.0 is the greatest possible value). This simply indicates that the fluctuations in discharge voltage and current are a consequence of the same physical phenomena.

The dashed curve in Figure 13 is for the cross correlation of the fluctuations of the discharge and beam currents. As the magnetic baffle current is varied from 6.0 to 12.0 amperes, the value of $R_{max}$ increased from 0.43 to 0.85 and then decreased to 0.21. This rather wide variation in the values of $R_{max}$ suggests that the dependence of the beam fluctuations on the discharge current fluctuations is strongest at the lower $J_{MB}$ values and is less elsewhere.

Figure 14 presents $R_{max}$, the maximum correlation coefficient, as a function of $J_B$, the beam current. The solid curve in Figure 14 is for the cross-correlations of the fluctuations of discharge voltage and current. As $J_B$ varies from 1.0 to 2.0 amperes, there is a slight variation in $R_{max}$. The high values of $R_{max}$ simply indicates, as previously noted, that the fluctuations in discharge voltage and current are a consequence of the same physical phenomena.

The dashed curve with square data symbols in Figure 14 is for the cross-correlations of the fluctuations of the discharge and beam currents. As the beam current increases from 1.0 to 2.0 amperes, the $R_{max}$ increases from 0.42 to 0.89. Because all of this data is taken at the lowest cathode flow rate consistent with the stable operation of the thruster subsystem, the increase in $R_{max}$ as $J_B$ increases is dependent on the $J_{MB}$ values. The fact that this is not a correlation of $J_E$ and $J_B$ fluctuations rather than the $J_I$ and $J_B$ fluctuations should not materially alter the results (see Appendix B). In Reference 6 the opposite trend of $R_{max}$ with increasing $J_B$ was obtained. This difference in the behavior of $R_{max}$ with $J_B$ has to be attributed to the differences in thruster geometry and power conditioning console in the two situations. It would be of interest to perform these experiments using a given thruster powered by several different power conditioning consoles.

The small-dashed curve with triangular data symbols in Figure 14 is for the cross correlations of the fluctuations of the neutralizer keeper and beam currents. For beam currents of 1.5 and 2.0 amperes the $R_{max}$ values are small and agree with those obtained in Reference 6. This lack of high correlation is in agreement with the fact that the two spectra are dissimilar in shape (i.e., for $J_B$ of 2.0 refer to Fig. 11). The rather high value, 0.69 for $R_{max}$ at $J_B$ of 1.0 is probably indicative of the low-frequency fluctuations of the neutralizer keeper supply having a significant effect on the spectrum of the beam fluctuations. Thus, the cross-correlation of these two fluctuations would have a high value of $R_{max}$. This increase in $R_{max}$ at $J_B$ of 1.0 is contrary to the results of Reference 6 wherein the $R_{max}$ values ranged from 0.12 to 0.19 for $J_B$ from 1.0 to 2.0 amperes.

## Concluding Remarks

An experimental investigation of the fluctuations of the discharge and beam plasmas of a 30-centimeter ion thruster has been performed. The power supplies were of the 60 hertz laboratory type. Studied were a range of beam currents, $J_B$,

from 1.00 to 2.00 amperes and a range of magnetic baffle currents, $J_{MB}$, from 6.0 to 15.0 amperes. Also studied were a small range of discharge currents and voltages about the optimum values for thruster operation at an energy expenditure of 185 electron volts per ion and a discharge voltage of 37.0 volts. The results include the following:

1. The beam current fluctuation intensity (defined as the ratio of the rms magnitude of the fluctuating to time-average currents) varied from 0.017 to 0.110.

2. The fluctuation intensity of the discharge current varied from 0.022 to 0.288.

3. The intensity of the fluctuations was found to depend significantly on the beam and magnetic baffle currents and the dependence on the latter current indicated that there were several plasma modes in evidence across the range of magnetic baffle current.

4. The intensity of the fluctuations was found not to depend significantly on the ranges of discharge voltage and current studied.

5. The shape of the spectra of the discharge plasma fluctuations was found to depend on both the beam and the magnetic baffle currents, but primarily on the latter and the dependence on the magnetic baffle current and beam current was found to be complex.

6. The predominant amplitudes of the spectra of the beam and discharge currents occurred at frequencies less than 30 kilohertz and the discharge chamber resonance could possibly be attributed to ion-acoustic wave phenomenon.

7. The cross-correlations of the discharge voltage and current fluctuations gave values of the maximum correlation coefficient which ranged from 0.70 to 0.85.

8. The cross-correlations of the discharge and beam currents indicated that the dependence on the magnetic baffle current was strong and highest at a magnetic baffle current about 1 ampere above that required for minimum cathode flow rate and stable thruster operation.

9. The cross-correlations of the fluctuations of the discharge and beam currents and the neutralizer keeper and beam currents were found to depend on the time-average beam current.

10. The results of the spectral and cross correlation measurements indicated (a) that the discharge current fluctuations directly contribute to the beam current fluctuations and (b) that there is some evidence that the power supply characteristics affect the fluctuations.

## Appendix A

## List of Symbols

| | |
|---|---|
| $A_0$ | relative amplitude of peak occurring at fundamental frequency, dimensionless |
| $A_1, A_2, \ldots$ | relative amplitude of peaks at first, second, . . . harmonic frequencies, dimensionless |
| $F_0$ | fundamental frequency, kHz |
| $F_1, F_2, \ldots$ | first, second, . . . harmonic frequencies, kHz |
| f | frequency, Hz |
| J(t) | $= \overline{J(t)} + j(t)$ sum of time-average and time-varying currents, A |
| $J_B(t)$ | beam current, A |
| $J_E(t)$ | emission current, A |
| $J_I(t)$ | discharge current, A |
| $J_{MB}$ | magnetic baffle current, A |
| $J_{NK}(t)$ | neutralizer keeper current, A |
| j(t) | time-varying current, A |
| $\dot{m}_c$ | equivalent neutralizer flow rate, mA |
| R | correlation coefficient as a function of $\tau$, the time-delay |
| $R_{max}$ | maximum correlation coefficient |
| $\Delta V_I(t)$ | $= \overline{\Delta V_I(t)} + \Delta v_I(t)$ sum of time-mean and time-varying discharge voltages, V |
| $\Delta v_I(t)$ | time-varying discharge voltage, V |
| $\tau$ | time-delay between two fluctuations |
| ' | fluctuation intensity defined as ratio of rms magnitude to time-average $\left(\text{i.e., } j'_B = \sqrt{\overline{j_B^2}}/\overline{J_B}\right)$ |
| — | overbar denotes time average of a physical quantity |

## Appendix B

## Effect of Screen Current on Measurements of Fluctuations

As indicated in the discussion of the results, the discharge current fluctuations were sensed rather than the fluctuations of emission current, $J_E$. The discharge current, $J_I(t)$ is

$$J_I(t) = J_E(t) + J_S(t) \qquad (B1)$$

where $J_S(t)$ is the screen current and further

$$J_S(t) = J_B(t) + J_A(t)$$

where $J_A(t)$ is the accelerator grid drain current. However, because

$$J_A(t) \ll J_B(t)$$

it follows that

$$J_S(t) \approx J_B(t)$$

Therefore, Equation (B1) becomes

$$J_I(t) = J_E(t) + J_B(t) \tag{B2}$$

$J_I(t)$ can be written as

$$J_I(t) = \overline{J_I(t)} + j_I(t) \tag{B3}$$

where $\overline{J_I(t)}$ is the time-average of $J_I(t)$ and $j_I(t)$ is the time-varying part. The same can be done for $J_E(t)$ and $J_B(t)$. Thus,

$$J_E(t) = \overline{J_E(t)} + j_E(t) \tag{B4}$$

$$J_B(t) = \overline{J_B(t)} + j_B(t) \tag{B5}$$

Using (B3), (B4), and (B5) and the fact that the time-average discharge current is

$$\overline{J_I(t)} = \overline{J_E(t)} + \overline{J_B(t)} \tag{B6}$$

gives the time-varying discharge current as

$$j_I(t) = j_E(t) + j_B(t) \tag{B7}$$

Taking the root-mean-square of both sides of equation (B7) and dividing by $\overline{J_I(t)}$ gives

$$j_I' = \frac{\sqrt{\overline{j_I^2(t)}}}{\overline{J_I(t)}} = \frac{\sqrt{\overline{j_E^2(t)}} + \sqrt{\overline{2j_E(t)j_B(t)}} + \sqrt{\overline{j_B^2(t)}}}{\overline{J_I(t)}} \tag{B8}$$

where $j_I'$ is defined as the fluctuation intensity for the discharge current. To assess more readily the effect of sensing $j_I(t)$ rather than $j_E(t)$, equation (B8) can be rewritten as

$$j_I' = \frac{\sqrt{\overline{j_E^2(t)}}}{\overline{J_E(t)}} + \frac{\sqrt{\overline{j_E^2(t)}}}{\overline{J_E(t)}}\left(\frac{\overline{J_E(t)}}{\overline{J_I(t)}} - 1\right) + \frac{\overline{J_E(t)}}{\overline{J_I(t)}}\left(\frac{\sqrt{\overline{2j_E(t)j_B(t)}}}{\overline{J_E(t)}} + \frac{\sqrt{\overline{j_B^2(t)}}}{\overline{J_E(t)}}\right) \tag{B9}$$

The form of Equation (B9) allows an evaluation of the differences between the fluctuation intensities, $j_I'$, and $j_E'$. In Equation (B4) the first term is $j_E'$. Thus, if the second and third terms are small, then $j_I' \approx j_E'$. The second term is small because $\overline{J_E(t)}/\overline{J_I(t)}$ has a value nearly one. For the third term there are two parts. The first part contains a factor $\overline{j_E(t)j_B(t)}$ which obviously depends linearly on $j_B(t)$. The second part of the third term contains a quadratic factor in $j_B(t)$. From the measurements it was found that $\sqrt{\overline{j_B^2(t)}} < \sqrt{\overline{j_I^2(t)}}$ and because $\overline{J_I(t)} > \overline{J_B(t)}$ by a factor of 6, it follows that for the results on fluctuation intensity presented herein, $j_I' \approx j_E'$.

To understand what are the differences for the cross correlations $\overline{j_I(t)j_B(t)}$ and $\overline{j_E(t)j_B(t)}$, consider the following:

$$R_{J_I,J_B}(\tau) = \frac{\overline{j_I(t)j_B(t+\tau)}}{\sqrt{\overline{j_I^2(t)}}\sqrt{\overline{j_B^2(t)}}} \tag{B10}$$

where $R_{J_I,J_B}(\tau)$ is the cross-correlation coefficient of the $j_I(t)$ and $j_B(t)$ and $\tau$ is a time-delay introduced between the two signals (see Appendix B, Ref. 6)

The results presented herein given as $R_{max}$ simply result from taking the maximum of the absolute value as

$$R_{max} = \left|R_{J_I,J_B}(\tau)\right|_{max} \tag{B11}$$

Using Equation (B7), Equation (B10) can be rewritten as

$$R_{J_I,J_B}(\tau) = \frac{\left[\overline{j_E(t)j_B(t+\tau)} + \overline{j_B(t)j_B(t+\tau)}\right]}{\sqrt{\overline{j_I^2(t)}}\sqrt{\overline{j_B^2(t)}}} \tag{B12}$$

Because from the measurements $j_B(t) < j_E(t)$ the second term in Equation (B12) is smaller than the first term. In addition, if it is noted that $\sqrt{\overline{j_I^2(t)}}\Big/\sqrt{\overline{j_E^2(t)}} \sim 1$, then

$$R_{J_I,J_B}(\tau) \approx R_{J_E,J_B}(\tau)$$

where $R_{J_E,J_B}(\tau)$ is the cross correlation coefficient for the emission current and beam current fluctuation.

The above analysis shows that, under the usual steady-state operating conditions of the thruster, sensing the discharge current fluctuations is essentially equivalent to sensing the emission current fluctuations. However, under abnormal conditions such as transients or high values of $J_A$, the above analysis is not valid.

## References


1. Duxbury, John H., "An Integrated Solar Electric Spacecraft for the Encke Slow Flyby Mission," AIAA Paper 73-1126, Lake Tahoe, Nev., 1973.

2. Gilbert, J. and Guttman, C. H., "The Evolution of the SEP Stage/SEPS/Concept," AIAA Paper 73-1122, Lake Tahoe, Nev., 1973.

3. Masek, T. D., Richardson, E. H. and Watkins, C. L., "Solar Electric Propulsion Stage Design," AIAA Paper 73-1124, Lake Tahoe, Nev., 1973.

4. "Thermoelectric Outer Planets Spacecraft (TOPS), JPL-TM-33-589, Apr. 1973, Jet Propulsion Laboratory, Pasadena, Calif.; also CR-131451, 1973, NASA.

5. Gardner, J. A., "Solar Electric Propulsion System Integration Technology (SEPSIT). Volume 1: Technical Summary," JPL-TM-33-583-Vol.-1, Nov. 1972, Jet Propulsion Laboratory, Pasadena, Calif.; also CR-130701, 1972, NASA.

6. Serafini, J. S. and Terdan, F. F., "Plasma Fluctuations in a Kaufman Thruster," Journal of Spacecraft and Rockets, Vol. 11, No. 11, Nov. 1974, pp. 752-758 (also AIAA paper 73-1056).

7. Serafini, John S., "Correlation Measurements of Plasma Fluctuations in a Hall-Current Accelerator," Bulletin of the American Physical Society, Vol. 13, No. 2, Feb. 1968, p. 278.

8. Serafini, J. S., "Utility of Conventional Turbulence Experimental Methods in the Study of Plasma Fluctuations," Bulletin of the American Physical Society, Vol. 13, No. 5, May, 1968, p. 824 (also TM X-52371, 1967, NASA).

9. Serafini, J. S., "Measurement of the Coherent Oscillations and Turbulence in Plasma Using Resistively and Capacitively Coupled Probes," TM X-1975, 1970, NASA.

10. Sovey, J. S. and King, H. J., "Status of 30 cm Mercury Ion Thruster Development," AIAA Paper 74-1117, San Diego, Calif., 1974.

11. Mantenieks, Maris and Rawlin, Vincent K., "Studies of Internal Sputtering on a 30-cm Thruster," AIAA Paper 75-400, New Orleans, La., 1973.

12. Finke, R. C., Holmes, A. D. and Keller, T. R., "Space Environment Facility for Electric Propulsion Systems Research," TN D-2774, 1965, NASA.

13. Poeschel, R. L., "The Variable Magnetic Baffle as a Control Device for Kaufman Thrusters," AIAA Paper 72-488, Bethesda, Md., 1972.

14. Kobayashi, M. and Takagi, A., "Oscillations in a Duoplasmatron Ion Source," Proceedings of the Second Symposium on Ion Sources and Formation of Ion Beams, Berkeley, Calif., Oct. 22-25, 1974.

15. Poeschel, R. L., "A 2.5 kW Advanced Technology Ion Thruster," August 1974, Hughes Research Labs., Malibu, Calif.; also CR-134687, 1974, NASA.

16. Cohen, A. J., "Onset of Anomalous Diffusion In Electron-Bombardment Ion Thruster," TN D-3731, 1966, NASA.

17. Wilbur, P. J., "Hollow Cathode Restartable 15 cm Diameter Ion Thruster," December 1973, Colorado State Univ., Fort Collins, Color.; also CR-134532, 1973, NASA.

Table 1. Amplitudes and frequencies of spectral peaks for discharge current fluctuations

| $J_{mb}$, | $F_0$, kHz/$A_0$ | $F_1$, kHz/$A_1$ | $F_2$, kHz/$A_2$ | $F_3$, kHz/$A_3$ | $F_4$, kHz/$A_4$ | $F_5$, kHz/$A_5$ |
|---|---|---|---|---|---|---|
| | | | (a) $J_b$ = 2.0 A | | | |
| 6.0 | 7.7/0.09 | 15.6/1.00 | 23.0/0.23 | 30.0/0.33 | 37.6/0.06 | |
| 7.0 | 8.9/0.04 | 18.0/1.00 | 27.1/0.22 | 36.5/0.16 | | |
| 8.5 | 9.8/0.26 | 19.3/1.00 | | 37.3/0.22 | | |
| 12.0 | 10.2/0.20 | 20.8/1.00 | 32.0/0.31 | 43.0/0.75 | | |
| | | | (b) $J_b$ = 1.5 A | | | |
| 7.0 | 10.3/1.0 | 20.4/0.70 | 30.3/0.25 | 41.2/0.13 | | |
| 9.0 | 8.0/0.15 | 15.7/1.0 | 23.5/0.24 | 39.5/0.07 | | |
| 11.0 | 8.6/0.69 | 17.0/0.95 | 25.5/1.00 | 33.8/0.98 | 42.3/0.67 | |
| 15.0 | 20.9/1.0 | 41.7/0.47 | | | | |
| | | | (c) $J_b$ = 1.0 A | | | |
| 8.0 | 9.8/1.0 | 19.4/0.47 | 29.2/0.25 | 38.8/0.25 | | |
| 9.0 | 4.7/0.12 | 9.1/1.0 | 13.5/0.27 | 17.8/0.57 | 22.3/0.55 | |
| 10.0 | 6.3/0.45 | 12.3/1.0 | 18.7/0.49 | 30.0/0.16 | | |
| 12.0 | 4.7/0.41 | 8.0/1.0 | 14.5/0.71 | 20.5/0.57 | 28.5/0.39 | |
| 15.0 | 6.7/0.57 | | 18.5/1.0 | | | 36.3/0.395 |

E-8234

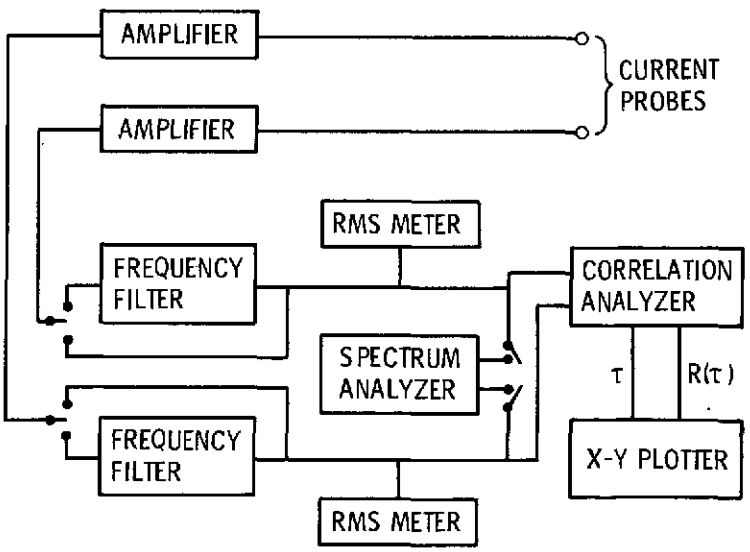


Figure 1. - Schematic diagram of instrumentation used to obtain cross-correlations and spectra for plasma fluctuations.

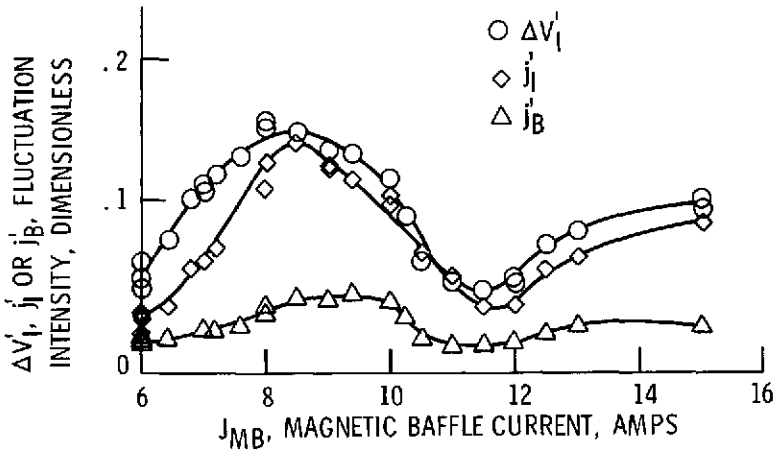


Figure 2. - Effect of varying the magnetic baffle current on the fluctuation intensity of the discharge current and voltage and ion beam current, $\overline{J}_B$ = 2.0 amps, $\overline{\Delta V_I}$ = 37.0 volts and $\overline{J}_I$ = 12.0 amps.

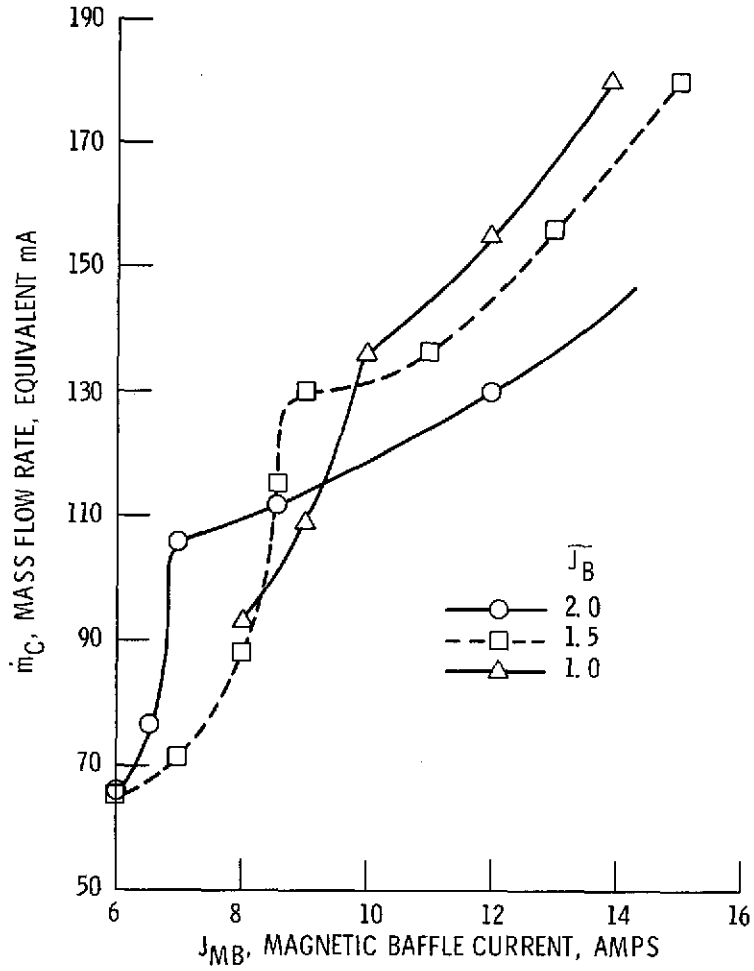


Figure 3. - Variation of cathode flow rate with magnetic baffle current for the 5.08 cm diameter baffle, $\overline{\Delta V_I}$ = 37.0 volts.

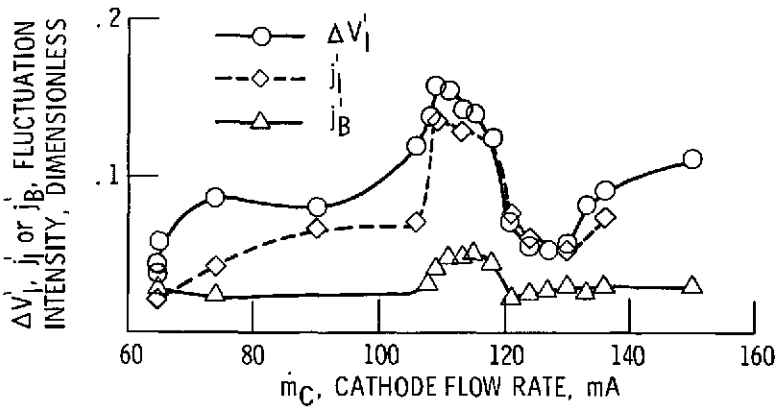


Figure 4. - Effect of varying the cathode flow-rate on the fluctuation intensity of the discharge voltage and current and beam current, $\bar{J}_B$ = 2.0 amps, $\overline{\Delta V_l}$ = 37.0 volts and $\bar{J}_l$ = 12.0 amps.



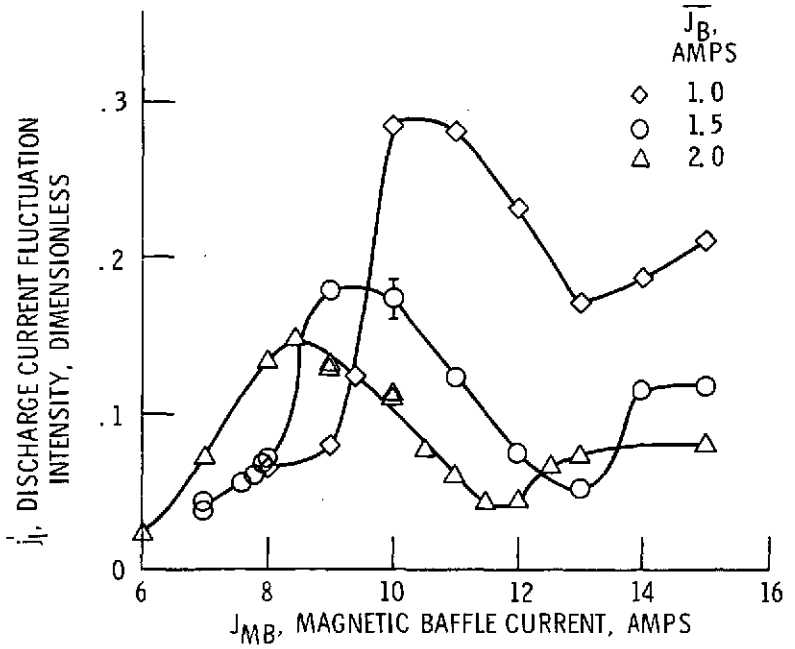


Figure 5. - Effect of varying the magnetic baffle current on the fluctuation intensity of the discharge current for $\bar{J}_B$ = 1.0, 1.5 and 2.0 amps with $\overline{\Delta V_l}$ = 37.0 volts.

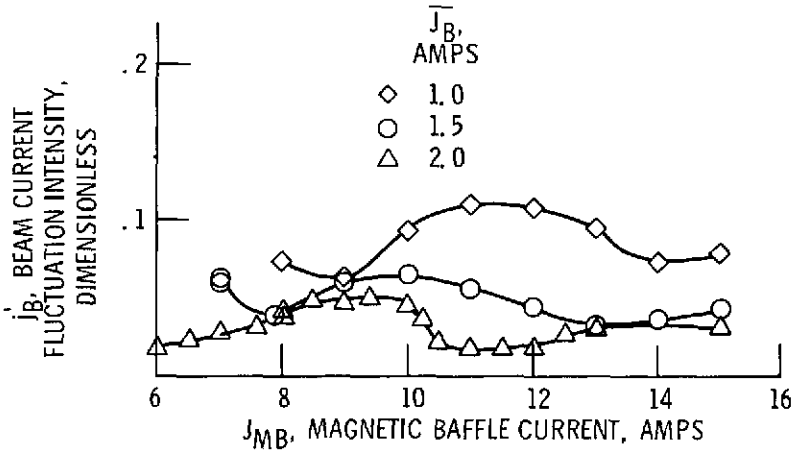


Figure 6. - Effect of varying the magnetic baffle current on the fluctuation intensity of the beam current for $\overline{J_B}$ = 1.0, 1.5 and 2.0 amps with $\overline{\Delta V_I}$ = 37.0 volts.

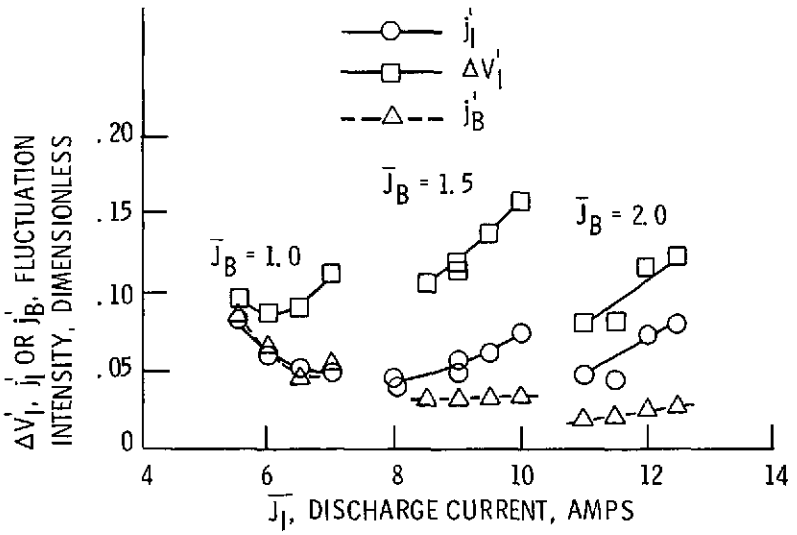


Figure 7. - Effect of varying discharge current on the fluctuation intensity of the discharge current and voltage and the beam current for $\overline{J_B}$ = 1.0, 1.5 and 2.0 amps with $\overline{\Delta V_I}$ = 37.0 volts and $J_{MB}$ = 8.0, 7.5 and 7.0 amps, respectively.

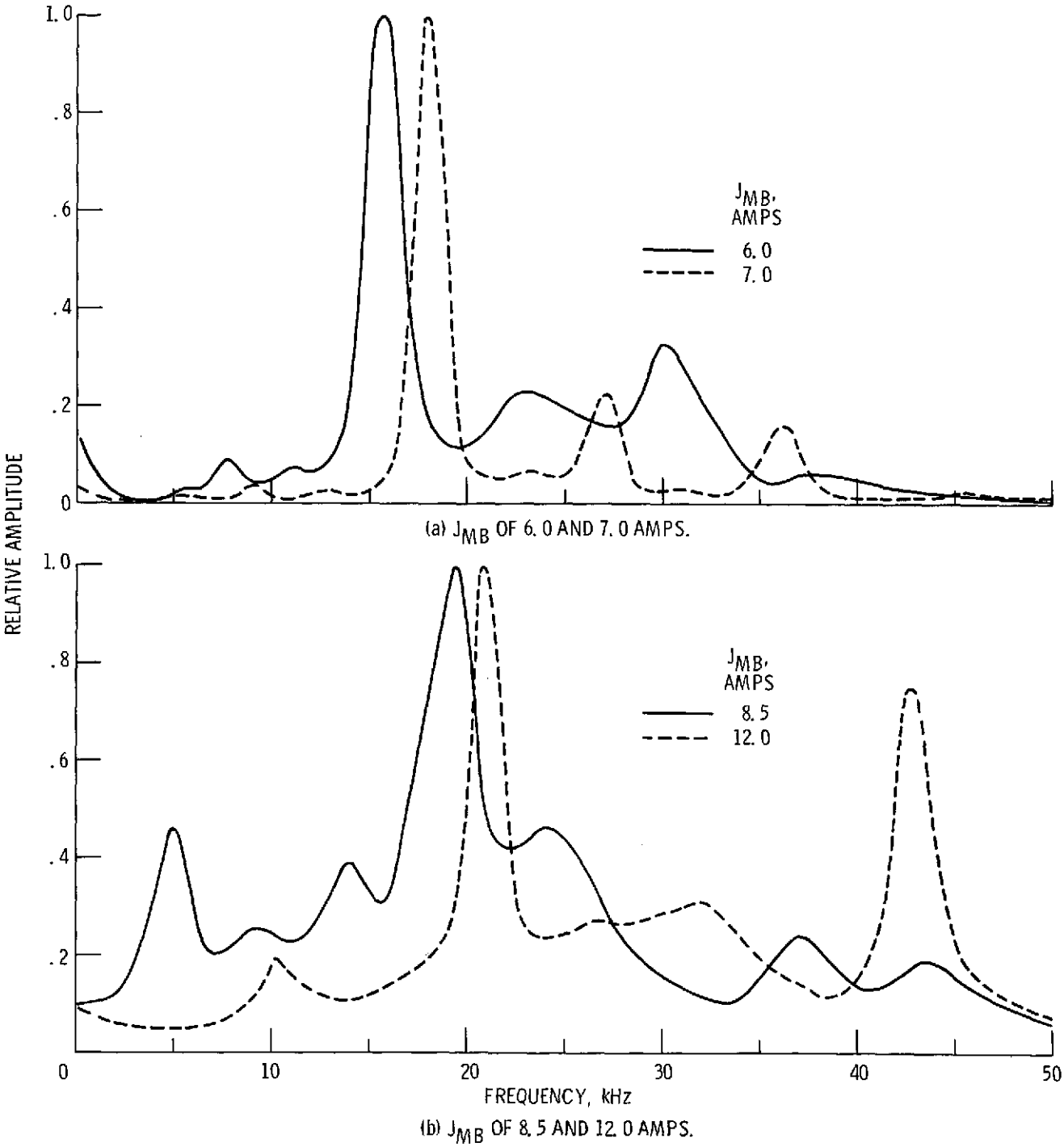


Figure 8. - Effect of various magnetic baffle currents on the relative amplitude as a function of frequency for the discharge current fluctuations with $\bar{J}_B$ = 2.0 amps, $\bar{J}_I$ = 12.0 amps and $\overline{\Delta V_I}$ = 37.0 volts.

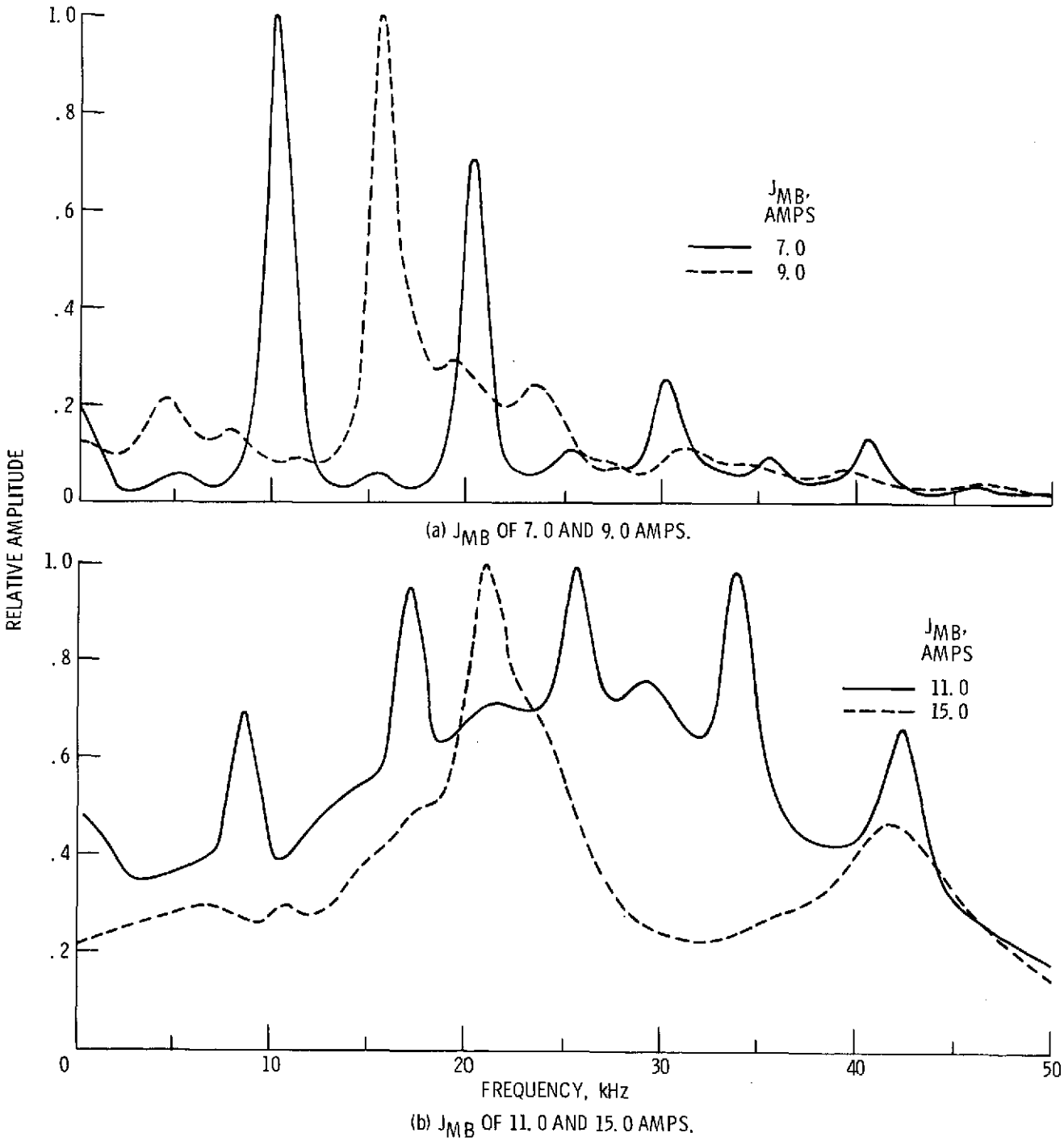


Figure 9. - Effect of various magnetic baffle currents on the relative amplitude as a function of frequency for the discharge current fluctuations with $\bar{J}_B$ = 1.5 amps, $\bar{J}_I$ = 9.0 amps and $\overline{\Delta V_I}$ = 37 volts.

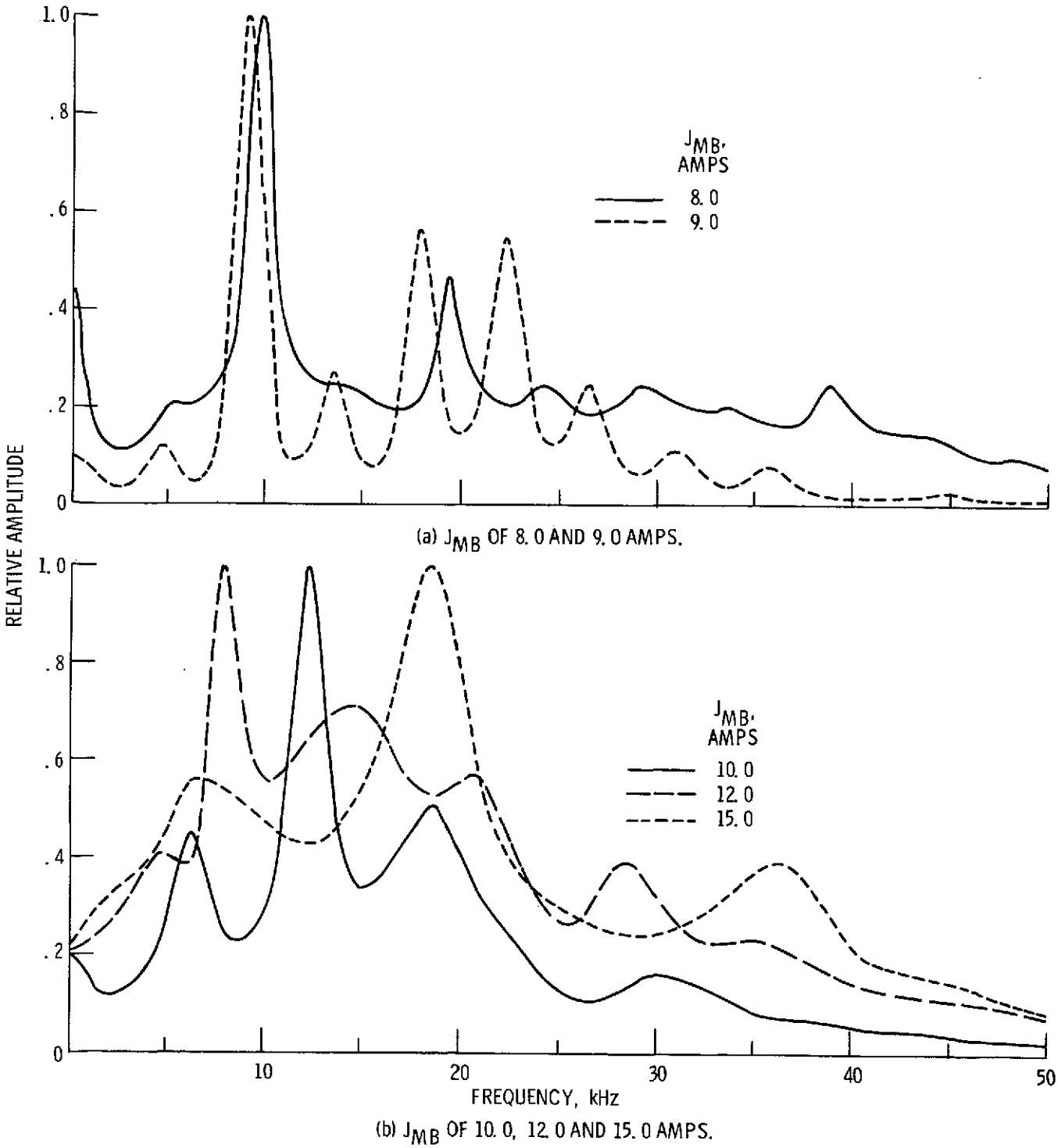


(a) $J_{MB}$ OF 8.0 AND 9.0 AMPS.

(b) $J_{MB}$ OF 10.0, 12.0 AND 15.0 AMPS.

Figure 10. - Effect of various magnetic baffle currents on the relative amplitude as a function of frequency for the discharge current fluctuations with $\overline{J_B}$ = 1.0 amps, $\overline{J_I}$ = 6.0 amps and $\overline{\Delta V_I}$ = 37.0 volts.

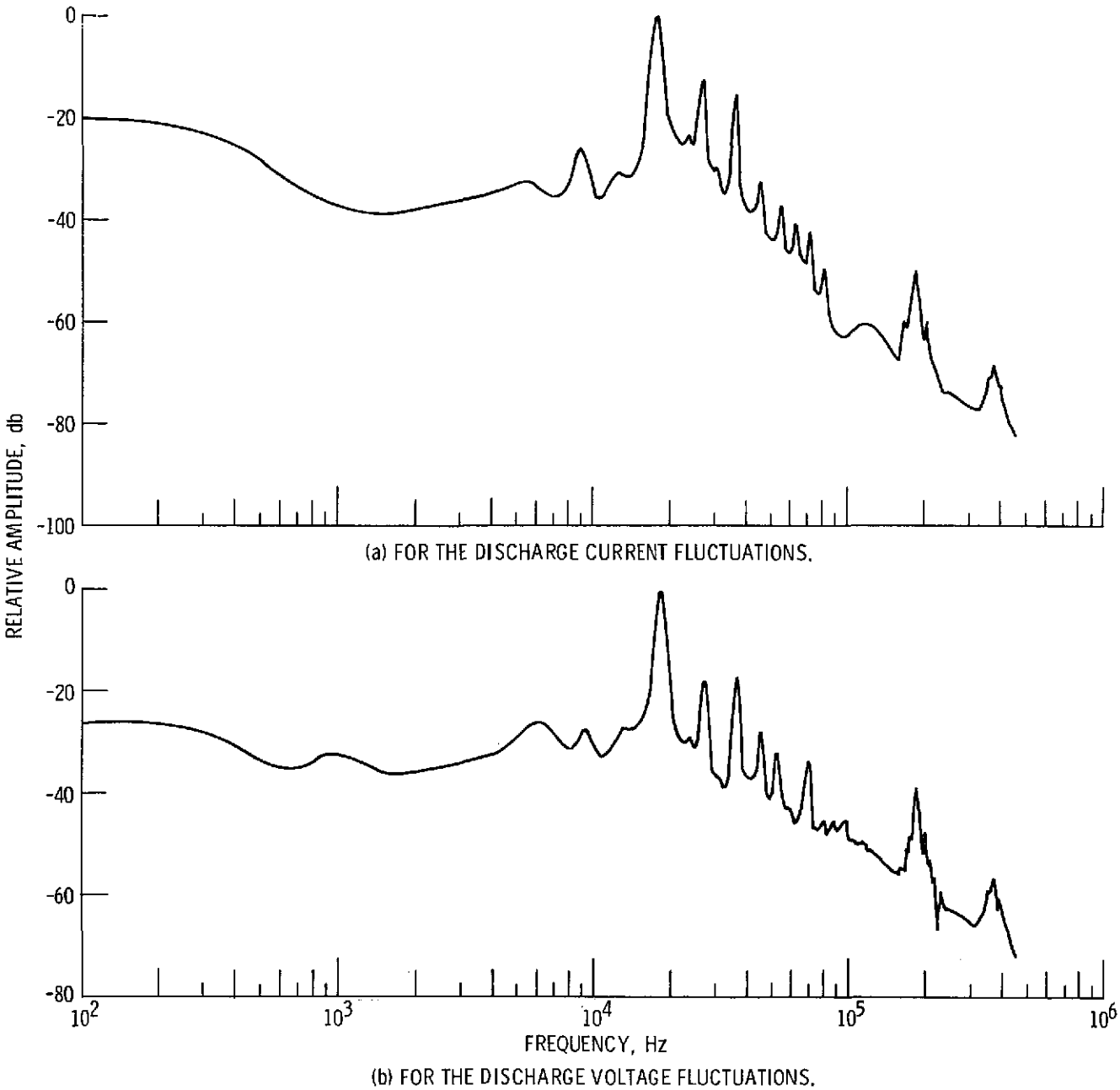


Figure 11. - Relative amplitude in decibels as a function of frequency for $\bar{J}_B$ = 2.0 amps, $\bar{J}_I$ = 12.0 amps and $\overline{\Delta V_I}$ = 37.0 volts.

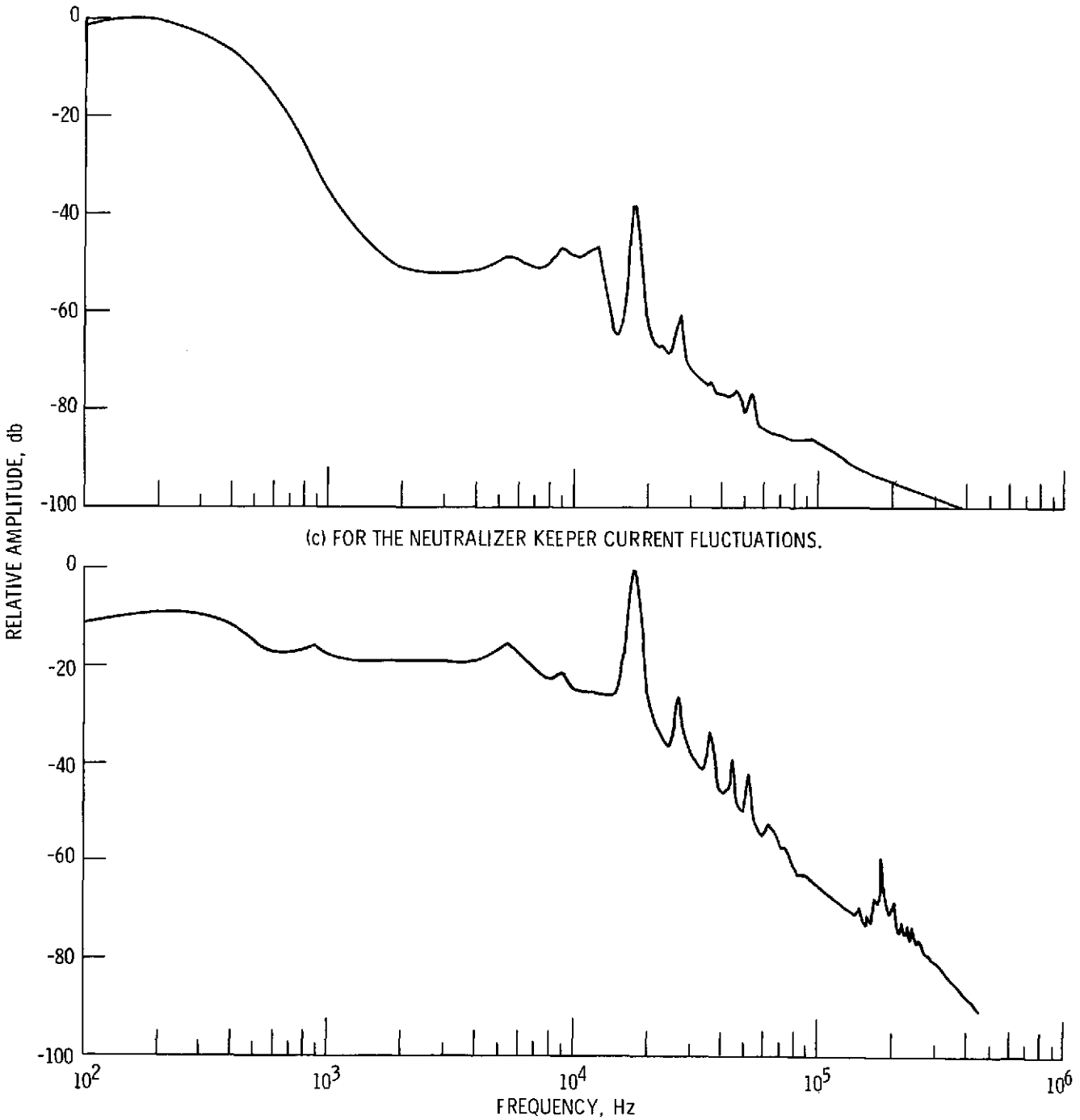


(c) FOR THE NEUTRALIZER KEEPER CURRENT FLUCTUATIONS.

(d) FOR THE BEAM CURRENT FLUCTUATIONS.

Figure 11. - Concluded.

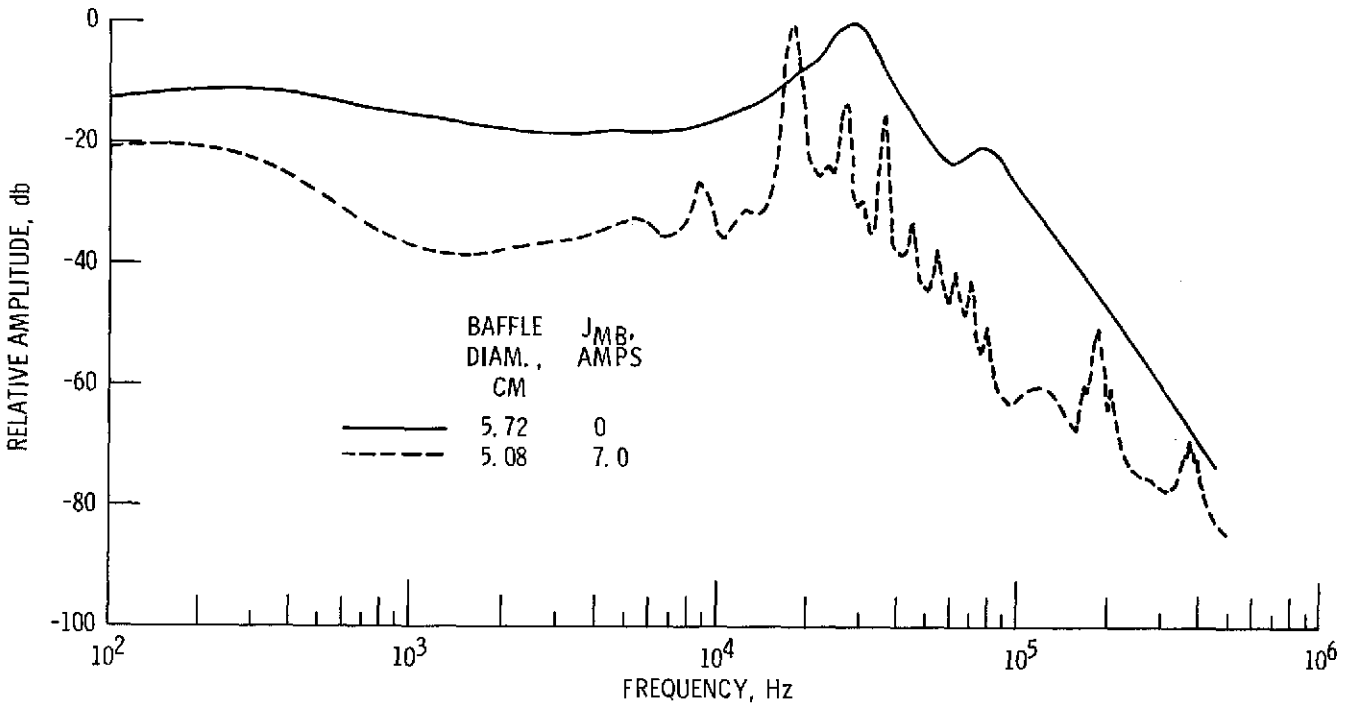


Figure 12. - Comparison of the relative amplitude in decibels as a function of frequency for the discharge current fluctuations for two different baffle diameters, $\bar{J}_B$ = 2.0 amps and $\overline{\Delta V_I}$ = 37.0 volts.

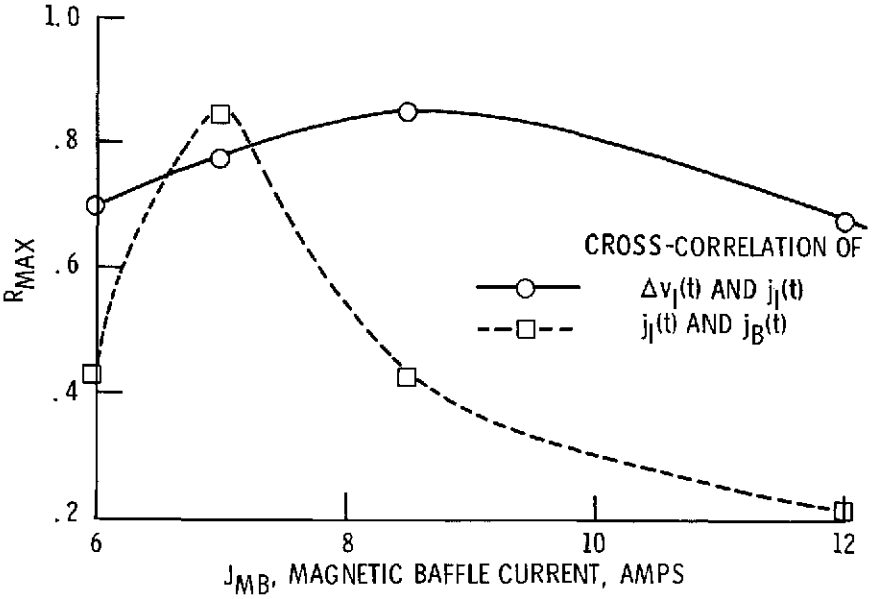


Figure 13. - Variation of $R_{max}$, maximum cross-correlation coefficient, as a function of magnetic baffle current, $J_{MB}$, for $\overline{J_B}$ = 2.0 amps, $\overline{\Delta V_I}$ = 37.0 volts and $\overline{J_I}$ = 12.0 amps.



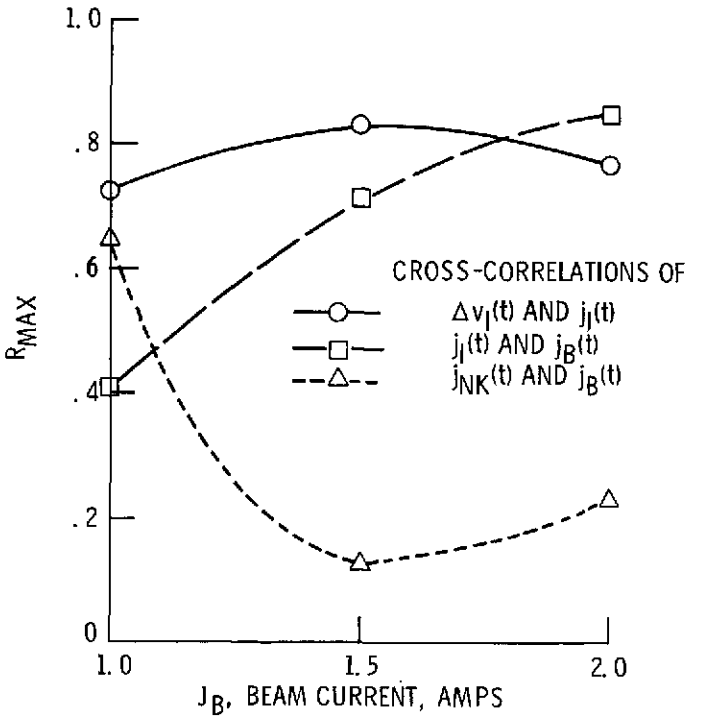


Figure 14. - Variation of $R_{max}$, maximum cross-correlation coefficient, as a function of the beam current, $\overline{J_B}$, for $\overline{\Delta V_I}$ = 37.0 volts and minimum cathode flow-rates.

NASA-Lewis